Observation of Detailed Structure of Turbulent Pulverized-Coal Flame by Optical Measurement*

(Part 1, Time-Averaged Measurement of Behavior of Pulverized-Coal Particles and Flame Structure)

Seung-Min HWANG**, Ryoichi KUROSE***, Fumiteru AKAMATSU****, Hirofumi TSUJI**, Hisao MAKINO** and Masashi KATSUKI****

The purpose of this study is to elucidate of the primary air combustion zone in pulverized-coal combustion by means of advanced laser-based diagnostics with high temporal and spatial resolutions. An open-type burner is fabricated to apply various optical measurement techniques. Detailed and overall evaluation is performed by applying various optical measurement techniques to the flame, such as the velocity and shape of nonspherical pulverized-coal particles, temperature, and light emissions from a local point in the flame. It is observed that the particle mean diameter increases as the distance from the burner increases, and this is found to be caused by the decrease in the diameters of small particles and the increase in the diameters of large particles, which result in the char reaction and the particle swelling due to devolatilization, respectively. The size-classified streamwise velocities of pulverized-coal particles in the central region of the jet exhibit the same magnitude, whereas those in the outer region are different depending on the particle size. The behavior is well explained in terms of the particle inertia.

Key Words: Pulverized-Coal Combustion, Shadow Doppler Particle Analyzer (SDPA), Laser Doppler Velocimetry (LDV), Two-Color Radiation Pyrometer

1. Introduction

Coal is an important and promising energy resource for electricity supply because its reserve is far more abundant than those of fossil fuels. At present, the major utilization method of coal in thermal power plants is pulverized-coal combustion, in which coal is pulverized into fine particles about 40 μm in mass median diameter[(1)–(3)]. The process of pulverized-coal combustion is a very complex phenomenon compared with that of gaseous or liquid fuel, since dispersion of coal particles, their devolatilization, and chemical reactions of volatilized fuel and residual char with air take place interactively at the same time[(4)]. Although it is estimated that various combustion modes coexist, since the particle sizes distribute widely from sub-micrometer to several hundreds of micrometers, the fundamental mechanism of pulverized-coal combustion has not been well understood. Therefore, new technologies about pulverized-coal combustion have still been developed empirically.

One of the reasons for the above-mentioned backgrounds is that it is very difficult to measure the instantaneous and simultaneous combustion fields in detail. The evaluations of the pulverized-coal combustion field in the furnace are mostly performed in the large-scale model burner corresponding to the boilers for power plants using invasive methods based on instruments such as a thermocouple and a gas sampling probe. When the probe is inserted directly in the flame, the flow field is disturbed

* Received 17th May, 2006 (No. 04-1257). Japanese Original: Trans. Jpn. Soc. Mech. Eng., Vol.71, No.710, B (2005), pp.2560–2567 (Received 22nd November, 2004)

** Energy Engineering Research Laboratory, Central Research Institute of Electric Power Industry (CRIEPI), 2–6–1 Nagasaka, Yokosuka, Kanagawa 240–0196, Japan. E-mail: hwangsm@criepi.denken.or.jp

*** Department of Mechanical Engineering and Science, Kyoto University, Yoshida-honmachi, Sakyo-ku, Kyoto 606–8501, Japan

**** Department of Mechanical Engineering, Osaka University, 2–1 Yamadaoka, Suita, Osaka 565–0871, Japan

and it is impossible to observe the detailed flame structure[5]–[14]. Combustion measurements based on optical diagnostics techniques, which allow noninvasive measurements of velocity, density, temperature, pressure and species concentration, have recently become of major interest. These techniques enable us to measure various physical properties with high temporal and spatial resolutions without distributing the flow field.

The purpose of this study is to apply advanced optical diagnostics to a pulverized-coal flame and to clarify the mechanism of pulverized-coal combustion in detail. For this purpose, a laboratory-scale pulverized-coal combustion burner is specially fabricated.

This study consists of two parts. In part 1, to investigate the time-averaged behavior of pulverized-coal particles and the flame structure, the velocity and shape of nonspherical pulverized-coal particles, temperature, and light emissions from a local point in the flame are measured by shadow Doppler particle analyzer (SDPA), two-color radiation pyrometer and specially designed light receiving optics (Multi-color Integrated Cassegrain Receiving Optics, MICRO), respectively. For SDPA, our research group[1] reported a study in which SDPA was applied to a turbulent pulverized-coal flame. However, the detailed structure of the pulverized-coal flame had not been well investigated. It showed only the applicability of SDPA to the pulverized-coal flame by measurement on the central axis of the flame. In part 2, planar laser-induced fluorescence (PLIF) is applied to the same flame, and instantaneous 2D measurements of the combustion reaction zone and the pulverized-coal particles are conducted[15].

2. Experiment Apparatus and Method

2.1 Pulverized-coal combustion burner

A turbulent pulverized-coal combustion burner is fabricated as an open-type apparatus to apply various types of optical measurement techniques. The burner and a series of supplying systems are illustrated schematically in Fig. 1. The burner has a coaxial structure having a main burner port (inner diameter: 6 mm) and an annular slit burner (width: 0.5 mm) installed outside of the main burner port. The main air supplied from a compressor is regulated to an assigned flow rate using a mass-flow controller. Pulverized-coal particles supplied and regulated by a screw feeder are sucked by the main air flow and mixed with the air in an injector to form a gas-solid two-phase jet issued from the main burner port.

In this study, methane is supplied to the annular slit burner installed outside of the main burner port to ignite the two-phase jet because the coal injection rate is very small and flame stabilization is impossible for a pure pulverized coal flame. Unburned pulverized coal particles in exhaust gas are collected by bag filters and exhaust gas is released into the atmosphere by a ventilator after cooling by a heat exchanger.

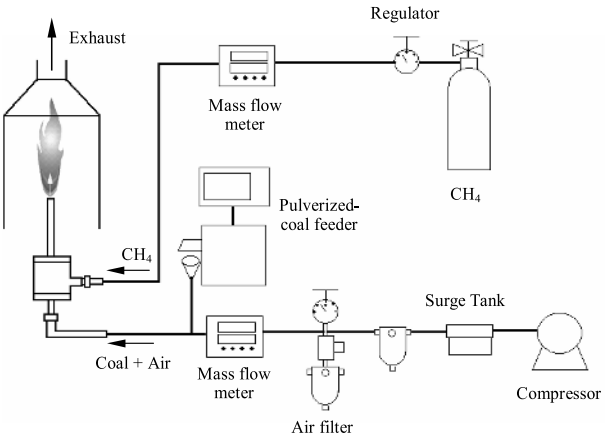

Fig. 1 Configuration of pulverized-coal burner and supply system

Table 1 Properties of coal

High heating value*1	29.1 MJ/kg
Low heating value*1	28.1 MJ/kg
Proximate analysis	[wt %]
Moisture*2	2.60
Ash*1	15.20
Volatile matter*1	26.90
Fixed carbon*1	57.90
Ultimate analysis	[wt %]
Carbon*1	71.90
Hydrogen*1	4.40
Nitrogen*1	1.5
Oxygen*1	6.53
Total sulfur*1	0.44
Combustible sulfur*1	0.39

*1 Dry basis, *2 As received

The coal we used is Newlands bituminous coal and this is pulverized under the same conditions as for actual pulverized-coal-fired power stations. The mass median diameter measured using a laser diffraction particle size analyzer is 33 μm. Table 1 shows the properties of Newlands coal.

2.2 Experimental method and conditions

In the experiment, first of all, the gas flame, to which air and methane are supplied to the main burner port and annular slit burner, respectively, is formed. The pulverized coal is supplied after the methane diffusion flame becomes stable, and the measurement is started when the pulverized-coal injection rate is regulated at 8.92 g/min. Table 2 shows the experimental conditions. The nominal bulk equivalence ratio, calculated on the basis of the mass ratio of the pulverized coal and the main air issued from the central burner port, is 6.09 which is a very high value. However, the pulverized-coal flame is of the open type, and it is considered that the nominal bulk equivalence is not important because not only the combustion with the coal, methane and air for the central burner port

Table 2 Experimental conditions

Pulverized-coal feed rate	1.49×10^{-4} kg/s
Air flow rate	1.80×10^{-4} m^3/s
CH_4 flow rate	2.33×10^{-5} m^3/s
Thermal input of coal*	4.19 kW
Thermal input of CH_4*	0.83 kW
Bulk equivalence ratio	6.09
Reynolds number	2544

* Based on low heating value

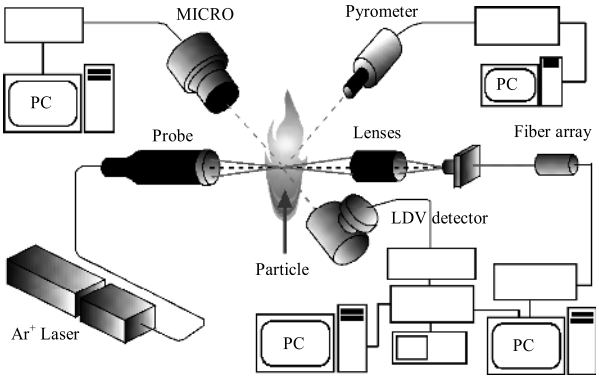

Fig. 2 Experimental setup

used for coal transportation but also the combustion induced by entrainment of ambient air occurs. The airflow rate for coal transportation is determined to avoid the deposition of coal particles in the air-supplying pipe. In addition, the nominal bulk equivalence ratio corresponds to that of the primary air combustion reaction zone in the actual pulverized-coal burners. Since the pulverized coal is not totally gasified at the exit of the burner port, it is considered that the actual local equivalence ratio is not so high. The methane flow rate is the minimum amount needed to form a stable flame. The origin for measurement is located at the center of the burner port, and z and r denote the axial and radial distances from the origin, respectively.

2.3 Optical measurement system

Various optical measurements are performed to comprehend the behavior of the pulverized-coal particles and the flame structure in the turbulent pulverized-coal flame. Figure 2 shows a schematic diagram of the measurement systems. In this study, the velocity and diameter of nonspherical pulverized-coal particles are measured simultaneously by SDPA[1)–4),16),17]. In SDPA measurement, however, velocity is obtained only when the diameter is measured correctly. Hence, the validity of velocity data obtained by SDPA should be assessed by comparing with laser Doppler velocimetry (LDV)[18),19)] measurement.

Ar^+ laser (NEC, GLG3282, effective output: 2 W (multiline oscillation)) light is divided into two laser beams by a beam splitter after the laser is separated to two wavelengths of 514.5 nm (green) and 488.0 nm (blue) by a color separator, and is transmitted to a transmission probe through an optical fiber. The parallel beam transmitted from the transmission probe is focused and crossed at the measurement point by a front lens (focal length: 500 mm). The laser light, scattered by particles passing on the measurement volume, is received by the LDV detector, and is transmitted to the LDV signal processor by an optical fiber. The scattering light is converted to photoelectrons in the LDV signal processor, and the particle velocity is calculated in the host computer. The particle image projected at the measurement volume is focused onto a one-dimensional photodiode array, and is converted to photoelectrons. The electric signal is converted into particle shape data in the SDPA signal processor and the equivalent circle diameter is calculated. The oscilloscope is used to verify the alignment of the LDV detector. In the noncombusting case, only the LDV measurement was conducted because the number density of coal particles was too high to conduct the SDPA measurement.

The two-color radiation pyrometer is used to measure the temperature of pulverized-coal particles. It is a temperature measurement system that receives the light of two different wavelengths ($\lambda_1 = 0.9\,\mu m$, $\lambda_2 = 1.0\,\mu m$) from the measured object using a sensor to obtain the ratio between the two wavelengths. Therefore, compared with a monochrome radiation pyrometer, it has the advantage that the measurement error due to changes in the radiation emissivity and view field is small.

On the other hand, to observe the time-averaged flame structure, the OH chemiluminescence (306 nm), CH band light emission (431.5 nm) and Mie scattering of coal particles (514.5 nm) from a local point of the pulverized-coal flame are measured by MICRO[20),21)]. An Ar^+ laser (wavelength = 514.5 nm) is used as the light source for the Mie scattering of coal particles. Since the flame light emission is overlapped on the peak wavelength of the optical interference filter for the Mie scattering of coal particles, the Mie scattering intensity is obtained as the difference between the intensities with and without the laser illumination. The light emissions and Mie scattering signals collected by MICRO are transmitted through the optical fiber, and detected and converted into a current signal by independent photomultipliers (PM's) through dichroic mirrors (DM's) and optical interference filters (F's) (F_{OH}: peak wavelength = 306 nm and half bandwidth = 10 nm, F_{CH}: peak wavelength = 431.5 nm and half bandwidth = 2 nm, F_{Mie}: peak wavelength = 516.5 nm and half bandwidth = 2 nm). Current signals from the photomultipliers are converted into a voltage signal by an I/V converter, and digitized by an A/D converter (DATEL, PCI-417G) at a sampling rate of 50 kHz.

3. Results and Discussion

3.1 Turbulent pulverized-coal flame

An example of a direct photograph of the pulverized-coal flame (exposure time: 1/8 000 sec) is shown in Fig. 3. The pulverized coal particles are visualized using an Ar^+ laser sheet inserted in the vicinity of the burner port. The photograph shows that the ignition of pulverized-coal particles starts in the vicinity of the burner port at $z = 30$ mm and combustion proceeds downstream to form a luminous flame. Table 3 shows the proximate analysis of Newlands coal after combustion. From the result, it is found that the combustion efficiency is 38.3% and that 44.6% of the volatile matter is emitted.

3.2 Change in velocity and diameter of pulverized-coal particles

Figure 4 (a) and (b) shows the axial distributions of the mean and rms (root mean square) velocities of pulverized-coal particles on the central axis of the burner. The comparison between the results in combusting and noncombusting cases shows that the mean velocity of the particles in the noncombusting case is markedly decreased with increasing axial distance, whereas the trend in the combusting case becomes gentle. This is due to the heat expansion of the gaseous phase caused by combustion reaction. On the other hand, rms velocity in the combusting case is small compared with that in the noncombusting case. It is considered that the turbulence of airflow is suppressed because the kinematic viscosity ascends with the decrease in airflow density as the temperature increases.

The radial distributions of the mean and rms velocities of pulverized-coal particles at axial distances of $z = 60$, 120 and 180 mm are shown in Fig. 5 (a) and (b), respectively. The mean velocity of pulverized-coal particles is highest on the central axis in every flame height and decreases gradually in the radial direction, following a Gaussian distribution. The gradient of velocity in the radial direction becomes gentle as the distance from the burner increases because the mean velocity of airflow decreases. In the noncombusting case, however, the mean velocity of particles is smaller than that in the combusting case at every flame height. As mentioned earlier, it is considered that this is due to the fact the heat expansion of the gaseous phase in the combusting case acts as an accel-

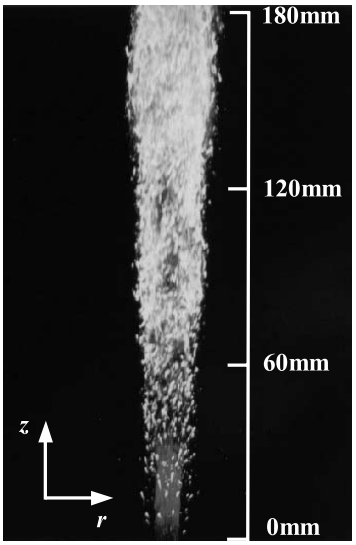

Fig. 3 Direct photograph of pulverized-coal flame

Table 3 Properties of coal (after combustion)

Proximate analysis	[wt %]
Moisture*2	3.40
Ash*1	19.10
Volatile matter*1	12.00
Fixed carbon*1	65.50

*1 Dry basis, *2 As received

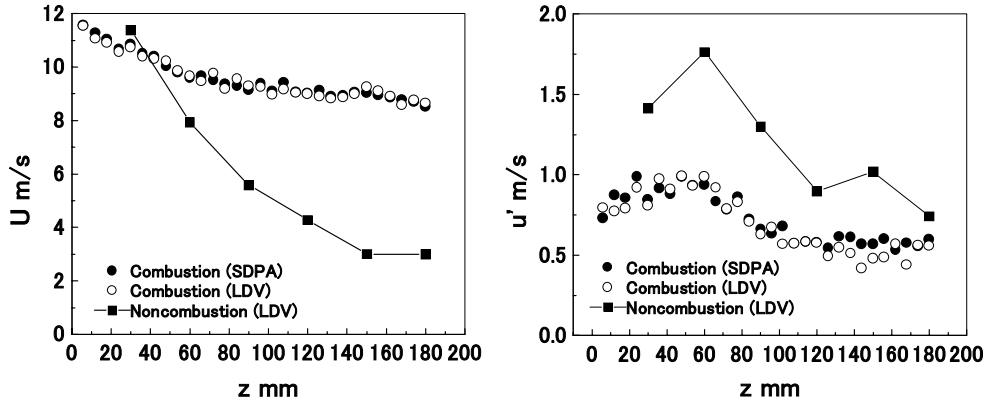

(a) Mean velocities (b) RMS velocities

Fig. 4 Axial distributions of mean and rms (root mean square) velocities of pulverized-coal particle determined by SDPA and LDV: (a) Mean velocities. (b) RMS velocities

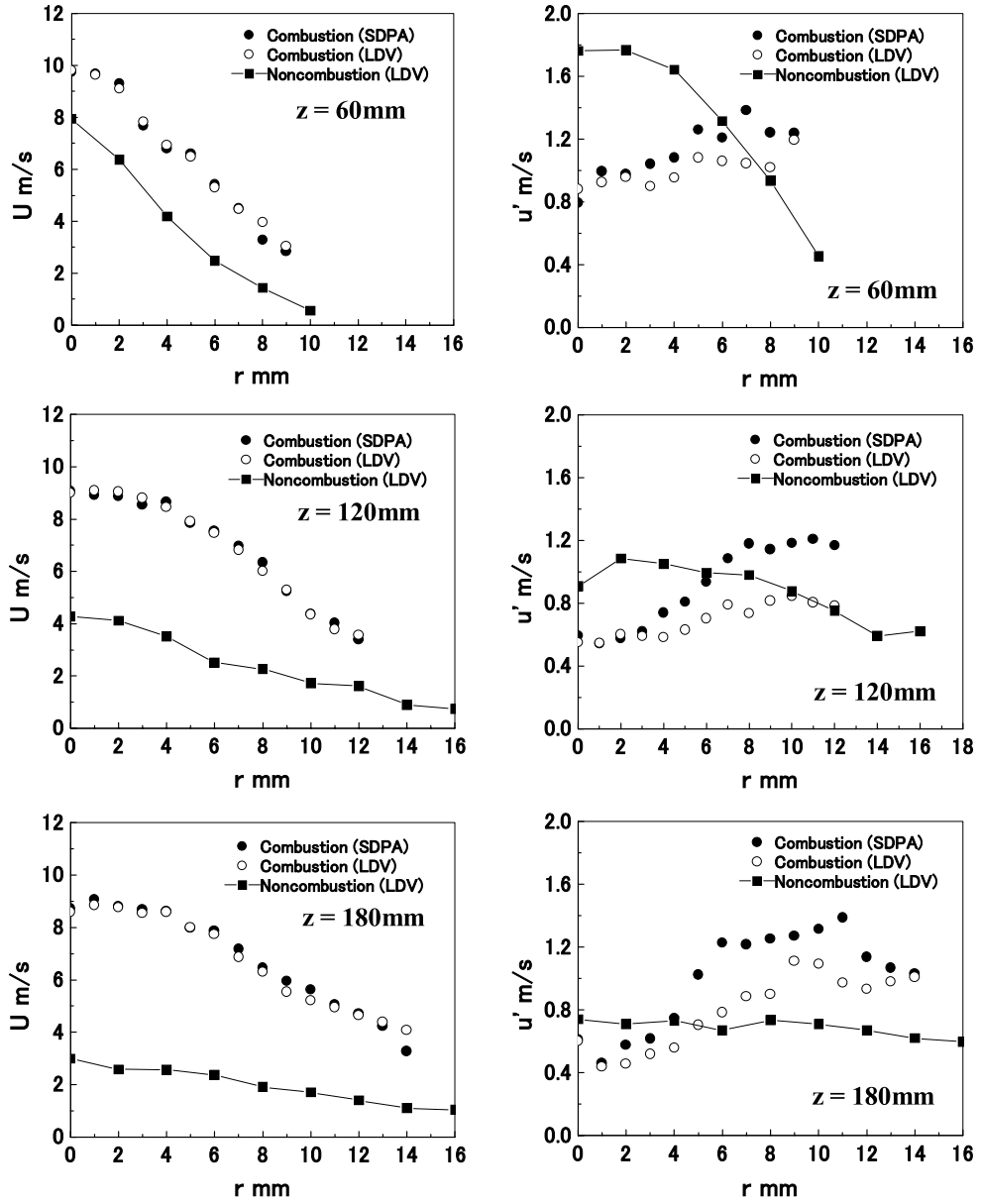

(a) Mean velocities (b) RMS velocities

Fig. 5 Radial distributions of mean and rms (root mean square) velocities of pulverized-coal particle determined by SDPA and LDV: (a) Mean velocities. (b) RMS velocities

erating force to the pulverized-coal particles. Concerning the rms velocity shown in Fig. 5 (b), on the other hand, the values in the vicinity of the central axis in the combusting case is small compared with those in the noncombusting case at every flame height because the turbulence is suppressed by the increase in kinematic viscosity. In the combusting case, however, the streamwise mean velocity is higher than that in the noncombusting case. Therefore, the rms velocity at the edge of the flame is high compared with that in the noncombusting case owing to entrainment of ambient air. It is also found that in the combusting case, the velocity data of SDPA is well consistent with that of LDV. This verifies that the accuracy of velocity measurement by SDPA is of the same level as in the case of LDV. For the radial distribution of rms velocity in Fig. 5 (b), however, the velocity measurement of SDPA is shown to be inconsistent with that of LDV. The difference between the two values of SDPA and LDV is considered to be due to the fact that the data rate of SDPA is low because the number density of pulverized-coal particles at the edge of the flame decreases extremely.

To investigate the behavior of pulverized-coal particles in more detail, the mean diameter (equivalent circle diameter), particle size distribution and circularity are considered using the result of simultaneous measurement of the particle velocity and shape by SDPA. The axial and

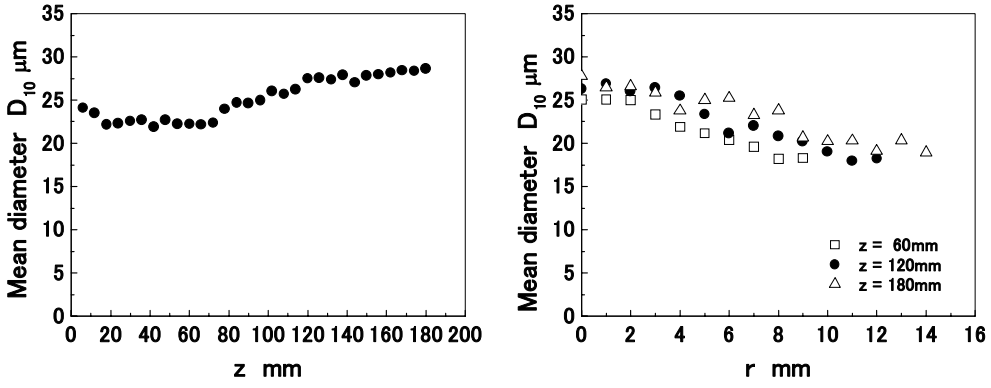

(a) Axial distribution (b) Radial distribution

Fig. 6 Mean diameter determined by SDPA: (a) Axial distribution. (b) Radial distribution

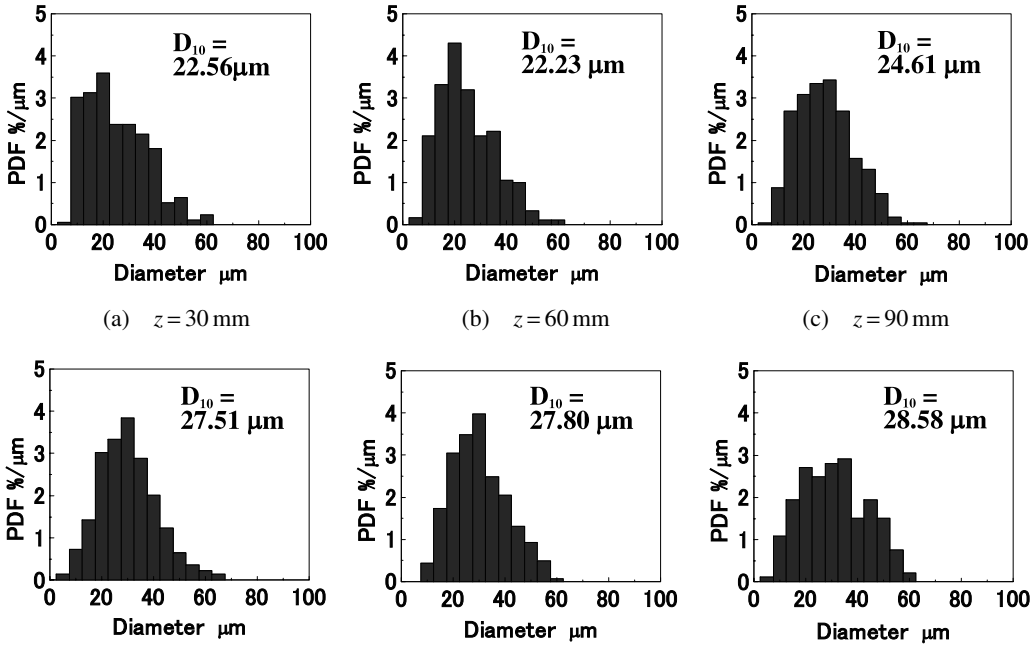

(a) $z = 30$ mm (b) $z = 60$ mm (c) $z = 90$ mm

(d) $z = 120$ mm (e) $z = 150$ mm (f) $z = 180$ mm

Fig. 7 Particle size distributions measured at $z = 30 \sim 180$ mm for every 30 mm on central axis of burner (the number base): (a) $z = 30$ mm, (b) $z = 60$ mm, (c) $z = 90$ mm, (d) $z = 120$ mm, (e) $z = 150$ mm, (f) $z = 180$ mm

radial distributions of the mean diameter of the pulverized-coal particles are shown in Fig. 6 (a) and (b), respectively. It is found that the mean diameter gradually increases as the distance from the burner increases, whereas it decreases as position is moved to edge of the flame.

To further investigate the reason for the increase in the mean diameter, the particle size distributions measured at $z = 30 \sim 180$ mm at 30 mm intervals on the central axis of the burner are shown in Fig. 7. Although there are a lot of particles with small diameters below 20 μm from the burner port to $z = 60$ mm, the peak is shifted to the large-diameter side as the distance from the burner increases. That is, it is speculated that the increase in the mean particle diameter is caused by the disappearance of small particles and the particle swelling due to devolatilization of volatile matter in the combustion process.

The particle size distributions on the radial direction at $z = 60$, 120, and 180 mm are shown in Fig. 8. It is found that the peak of the particle diameter distribution is shifted to the small-diameter side with increasing radial distance at every flame height. This is considered to be due to the fact that the particles with small diameters, which easily follow the airflow, tend to move away from the flame owing to the effect of turbulent organized motions and heat-induced expansion of the gaseous phase. In particular, it is found that the probability density of

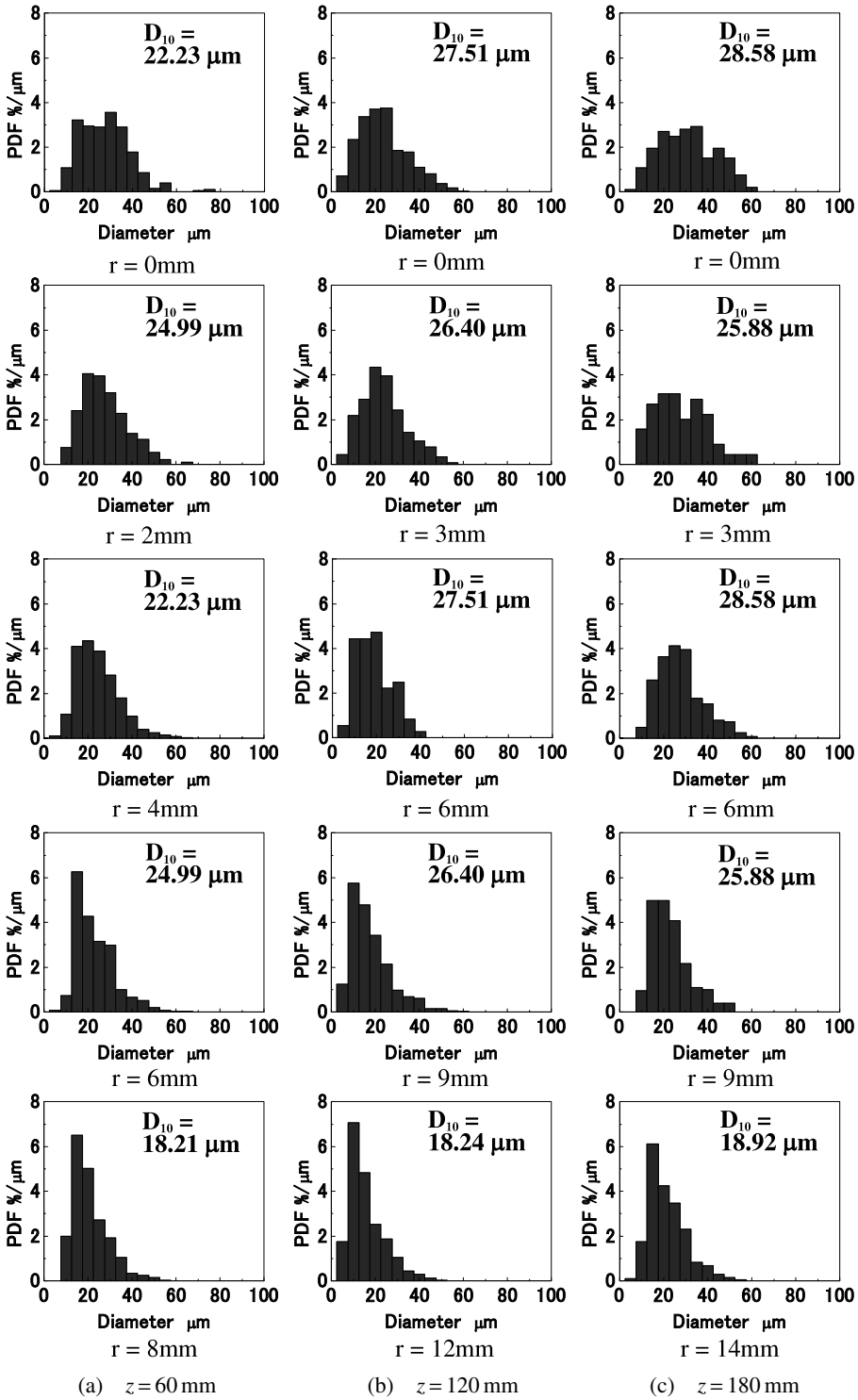

Fig. 8 Particle size distributions in radial direction ($z = 60$, 120 and 180 mm): (a) $z = 30$ mm, (b) $z = 60$ mm, and (c) $z = 90$ mm

particle diameters smaller than 20 μm becomes large as the radial distance increases. Saitoh et al.[22] applied the phase Doppler anemometer (PDA) measurement to polydisperse premixed-spray flames in a stagnation flow, and investigated the followability of fuel droplets in the airflow. According to the result, it is reported that if the droplet diameter is smaller than 20 μm, the followability in the gaseous-phase flow is concluded to be good. From these results, it is considered that particles smaller than 20 μm also have good followability in the gaseous-phase flow in the case of pulverized-coal-like droplets in spray combustion.

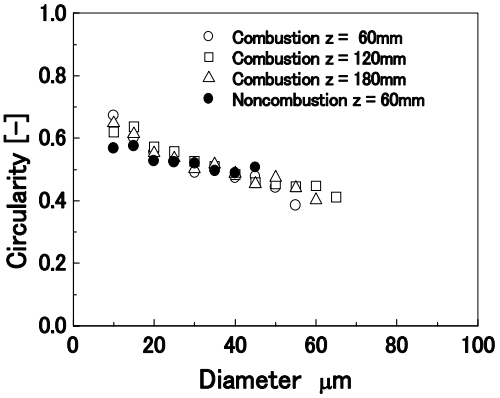

Fig. 9 Circularity as function of particle size in steps of 5 μm (z = 60, 120 and 180 mm, center position)

The various phenomena and characteristics of powder greatly depend on particle shape as well as particle size. In this study, the circularity[1),(23)], which is one of the most important indices for characterizing the particle shape, is examined. The circularity C ($0 < C < 1$) is an index that gives 1 for a true circle and 0 for a needle shape, and is calculated as follows:

$$C = \frac{\sqrt{4\pi A}}{c}, \tag{1}$$

where A and c are the cross-section area and circumferencial length of a particle, respectively.

The circularity was calculated at three points of z = 60, 120, and 180 mm on the burner central axis in the combusting case. In the noncombusting case, the SDPA measurement could not be carried out because of the high number density of particles. Hence, the measurement in the noncombusting case was performed at a number density lower than that in the combusting case only at one point of z = 60 mm. Figure 9 shows the circularity for particles of 5 μm size class at three locations. In the noncombusting case, the circularity of a particle over 40 μm could not be evaluated since the particle number is small and changes slightly. Although in both the combusting and noncombusting cases, the circularity decreases with increasing particle size, the decrease is marked in the combusting case. It is considered that, in the combusting case, the circularity of the large particles is increased owing to the crack and breakup caused by swelling, and that the circularity of small particles decreases owing to char reaction and melting.

To further investigate the behavior of pulverized-coal particles, the pulverized-coal particles were size-classified into every 5 μm range, and the velocity field of the particles for every size class was examined. Figure 10 (a) shows the size-classified mean and rms axial velocities of pulverized coal particles on the central axis at the distances of z = 60, 120, and 180 mm from the burner. The mean and rms velocities of pulverized-coal particles are independent of the particle size, and almost constant at every flame height. From this result, it is found that the mean and rms velocities of pulverized-coal particles at the center (r = 0 mm) are independent of the particle size.

Figure 10 (b) shows the size-classified mean and rms axial velocities of pulverized-coal particles on the edge at the distances of z = 60, 120, and 180 mm from the burner. However, in contrast to the results at the central position of the flame, it is confirmed that the mean and rms axial velocities of pulverized-coal particles highly depend on the particle size at every flame height. As the reason for this, it is considered that the particles in the central high-speed region tend to be pushed outwards owing to the thermal expansion of the gas phase and the organized motions that appear in the jet. Although the axial velocity of the small particles being pushed outwards is quickly decreased by the ambient fluid with decreasing velocity, that of the larger particles is not affected by the ambient fluid because of the their larger inertia. Therefore, the velocities of the large particles are higher than those of small particles on the edge of the flame.

3.3 Temperature distribution

Figure 11 shows the axial profile of mean temperature obtained using the two-color radiation pyrometer. The temperature is measured at $z = 6 \sim 180$ mm. However, the temperature data at $z < 18$ mm is not measured because temperature measurement was impossible in the vicinity of the burner port owing to the weak combustion reaction. The temperature of pulverized-coal particles shows a maximum value of 1 800°C at z = 30 mm and decreases gradually with increasing axial distance z. According to other studies[24),(25)], the heating rates of the pulverized coal in a furnace are on the order of 10^4 deg/sec. However, the present value becomes a much larger value on the order of 10^6 deg/sec. This is because the methane flame is used to ignite the pulverized-coal particles in this study.

It is difficult to define the temperature obtained by two-color pyrometer measurements, since this value is strongly affected by soot and gaseous species. Moreover, strictly speaking, this is not the value at a local point. It can be said that this temperature is the overall temperature for coal particles, soot, and gaseous species in a relatively large region. However, the obtained data is valuable not only for elucidating the detailed structure of pulverized-coal combustion but also for the assessment of the numerical simulations of two-phase combustions such as pulverized-coal and spray combustions.

3.4 Light emission intensity

The axial intensity profiles of the OH chemiluminescence, CH-band light emission and Mie scattering of coal particles measured from a local point in the pulverized-coal flame by MICRO are shown in Fig. 12 to observe the time-averaged flame structure. The intense OH chemiluminescence and CH band light emission detected near the burner below z = 20 mm is caused by the methane

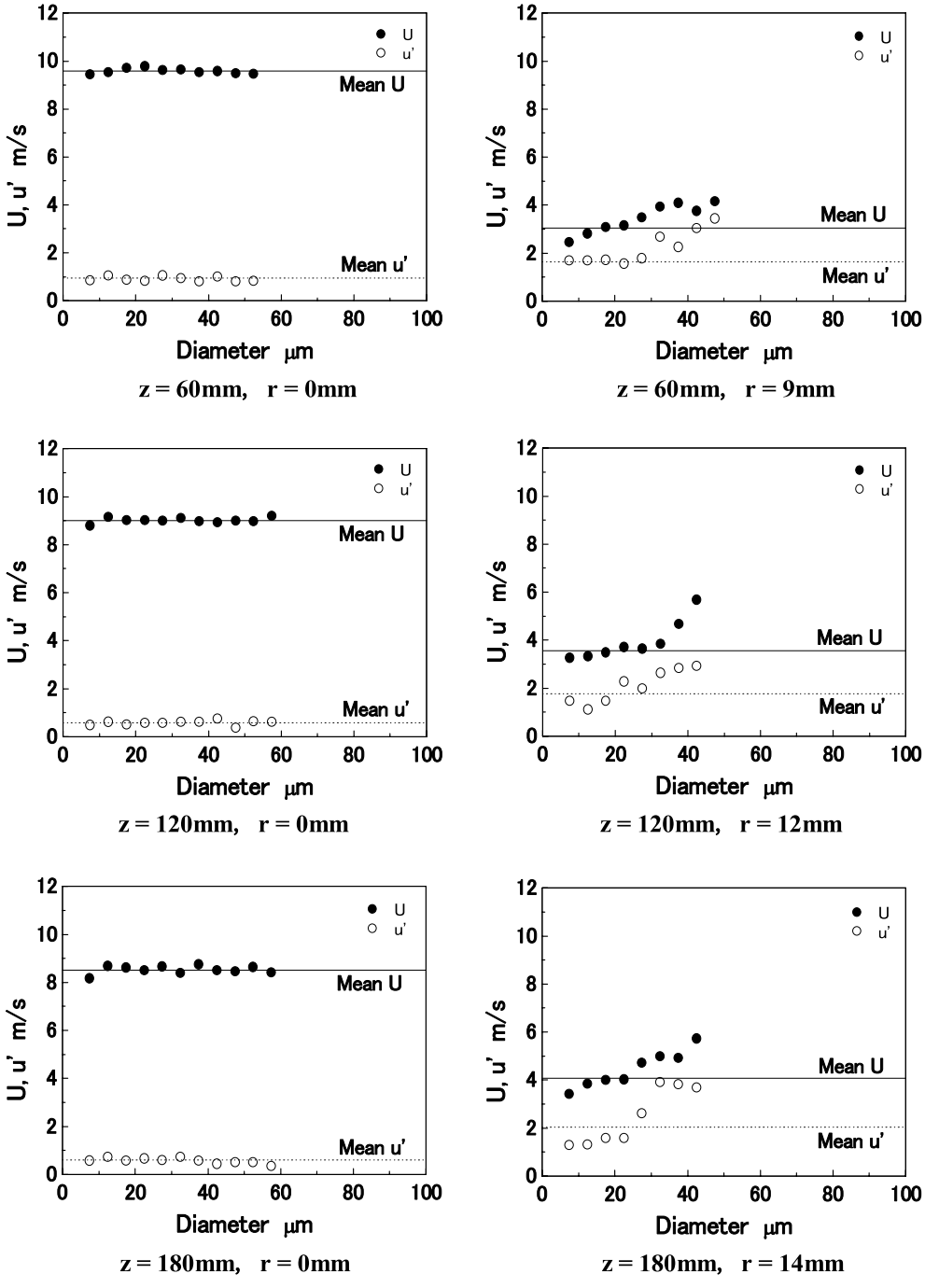

(a) Center position (b) Edge position

Fig. 10 Mean and rms particle velocities as function of particle size in steps of 5 μm ($z = 60$, 120 and 180 mm)

pilot flame. It is considered that the ignition starts in the region, where the Mie scattering intensity decreases rapidly from approximately $z = 40$ mm and the intensities of the OH chemiluminescence and CH-band light emission begin to rise again. Furthermore, the OH chemiluminescence intensity increases gradually from approximately $z = 40$ mm. CH band light emission intensity, on the contrary, increases markedly compared with that of OH chemiluminescence. This is considered to be due to the fact that the flame luminescence is increased as the combustion process proceeds as shown in Fig. 3 and the continuous spectrum accompanied with the solid-body radiation from soot is overlapped with that corresponding to the CH band emission.

Figure 13 shows the radial intensity profiles of the OH chemiluminescence, CH-band light emission, and Mie

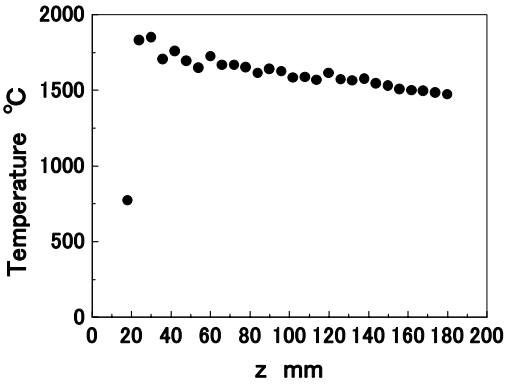

Fig. 11 Distribution of temperature on central axis obtained by two-color radiation pyrometer

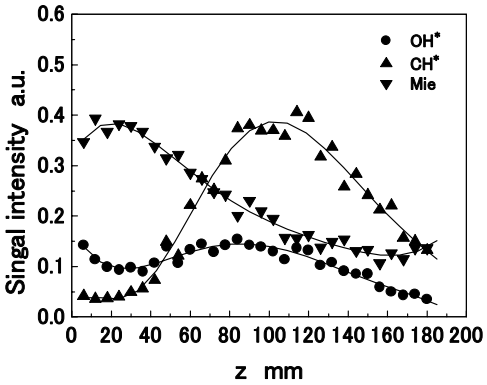

Fig. 12 Distributions of OH chemiluminescence and CH-band light emission from flame and Mie scattering intensity of pulverized-coal in z direction obtained by MICRO

scattering of coal particles measured at $z = 60$, 120, and 180 mm. The intensities of the OH chemiluminescence and CH-band light emission are higher in the outer region (approximately $r = 4 \sim 6$ mm) than those in the central region of the flame because the combustion reaction actively takes place owing to the mixing of coal particles with ambient air. It is also found that Mie scattering intensity decreases with increasing radial distance because the number density of the pulverized-coal particles is small in the outer region of the flame.

4. Conclusions

Precise optical diagnostics were applied to a laboratory-scale turbulent pulverized-coal flame, and the time-averaged behavior of the pulverized-coal particles and flame structure was examined. The main results obtained in this study can be summarized as follows.

(1) The mean velocity of the particles in the combusting case decreases gradually compared with that in the noncombusting case owing to the heat expansion of the gaseous phase caused by the combustion reaction. The rms velocity in the combusting case, on the other hand, is smaller than that in the noncombusting case because the turbulence of airflow is suppressed owing to the decrease in kinematic viscosity induced by the decrease in airflow density as the temperature increases.

(2) The size-classified mean and rms velocities of pulverized-coal particles in the central region of the flame are almost constant at every flame height and independent of the particle size. In the edge region of the flame, on the other hand, the mean and rms axial velocities of pulverized-coal particles highly depend on the particle size at every flame height.

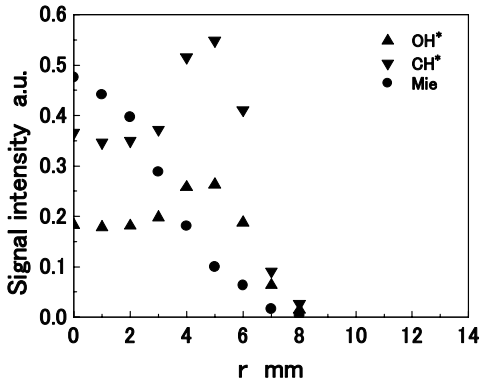

(a) $z = 60$ mm

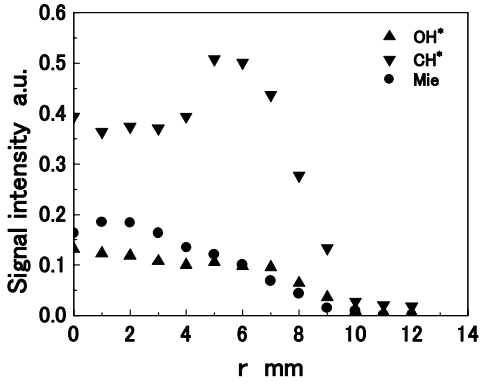

(b) $z = 120$ mm

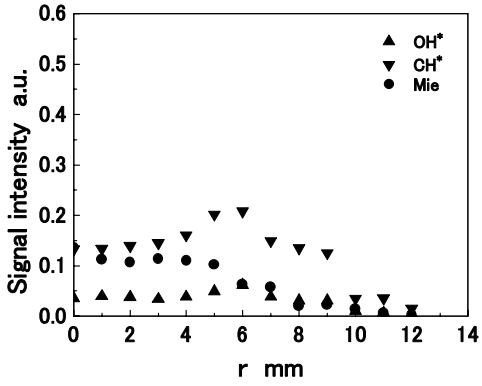

(c) $z = 180$ mm

Fig. 13 Distributions of OH chemiluminescence and CH-band light emission from flame and Mie scattering intensity of pulverized-coal in r direction obtained by MICRO: (a) $z = 30$ mm, (b) $z = 60$ mm, and (c) $z = 90$ mm

(3) For the circularity, which is one of the most important indices for characterizing the particle shape in both the combusting and noncombusting cases, the circularity decreases with increasing particle size, the decrease is marked in the combusting case. As a reason for this, it is considered that, in the combusting case, the circularity of the large particles is increased owing to the crack and breakup caused by swelling, and that the circularity of small particles decreases owing to char reaction and melting.

(4) The time-averaged value of flame luminescence can be a very effective index for evaluating the combustion characteristic of the flame. However, the time-averaged evaluation of the flame structure is not enough to discuss the instantaneous flame structure in detail.

Acknowledgements

The authors would like to thank Dr. Hiromi Shirai and Dr. Michitaka Ikeda of CRIEPI for many useful discussions.

References

(1) Tsuji, H., Kurose, R. and Makino, H., Simultaneous Measurement of Particle Velocity, Particle Shape and Particle Size in Pulverized Coal Flame by Shadow Doppler Velocimetry, Trans. Jpn. Soc. Mech. Eng., (in Japanese), Vol.68, No.666, B (2002), pp.569–602.

(2) Hwang, S.M., Kurose, R., Oomagari, K., Akamatsu, F., Tsuji, H., Makino, H. and Katsuki, M., Observation of the Detailed Structure of a Turbulent Pulverized Coal Combustion Flame, Proc. 4th Asia-Pacific Conf. on Combust., (2003), pp.414–417.

(3) Hwang, S.M., Kurose, R., Oomagari, K., Akamatsu, F., Tsuji, H., Makino, H. and Katsuki, M., Experimental Study on the Particle Behaviors and the Structure of a Turbulent Pulverized Coal Flame, Proc. Int. Conf. on Power Eng.-03, Vol.2 (2003), pp.393–398.

(4) Kurose, R., Akamatsu, F. and Makino, H, J. Soc. of Powder Tech. Jpn., (in Japanese), Vol.41, No.2 (2004), pp.114–123.

(5) Wang, F., Wang, X.J., Ma, Z.Y., Yan, J.H., Chi, Y., Wei, C.Y., Ni, M.J. and Chen, K.F., The Research on the Estimation for the NO_x Emissive Concentration of the Pulverized Coal Boiler by the Flame Image Processing Technique, Fuel, Vol.81 (2002), pp.2113–2120.

(6) Yin, C., Caillat, S., Harion, J., Baudoin, B. and Perez, E., Investigation of the Flow, Combustion, Heat-Transfer and Emission from a 609 MW Utility Tangentially Fired Pulverized-Coal Boiler, Fuel, Vol.81 (2002), pp.997–1006.

(7) Yan, Y., Lu, G. and Colechin, M., Monitoring and Characterization of Pulverized Coal Flames Using Digital Imaging Techniques, Fuel, Vol.81 (2002), pp,647–656.

(8) Sabel, T., Unterberger, S. and Hein, K.R.G., Application of Quotient Pyrometry to Industrial Pulverized Coal Combustion, Experimental Thermal and Fluid Sci., Vol.26 (2002), pp.283–289.

(9) Seames, W.S., An Initial Study of the Fine Fragmentation Fly Ash Particle Mode Generated during Pulverized Coal Combustion, Fuel Proc. Tech., Vol.81 (2003), pp.109–125.

(10) Spinti, J.P. and Pershing, D.W., The Fate of Char-N at Pulverized Coal Conditions, Combust. Flame, Vol.135 (2003), pp.299–313.

(11) He, R., Suda, T., Takafuji, M., Hirata, T. and Sato, J., Analysis of low NO Emission in High Temperature Air Combustion for Pulverized Coal, Fuel, Vol.83 (2004), pp.1133–1141.

(12) Nimmo, W., Patsias, A.A., Hampartsoumian, E., Gibbs, B.M. and Williams, P.T., Simultaneous Reduction of NO_x and SO_2 Emissions From Coal Combustion by Calcium Magnesium Acetate, Fuel, Vol.83 (2004), pp.149–155.

(13) Wei, X., Xu, T. and Hui, S., Burning Low Volatile Fuel in Tangentially Fired Furnaces with Fuel Rich/Lean Burners, Energy Conservation and Management, Vol.45 (2004), pp.725–735.

(14) William, J.O., Richard, A.H., Evan, J.G. and Henry, W.R., Recent Advances in Mercury Removal Technology at the National Energy Technology Laboratory, Fuel Proc. Tech., Vol.85 (2004), pp.533–548.

(15) Hwang, S.M., Kurose, R., Akamatsu, F., Tsuji, H., Makino, H. and Katsuki, M., Observation of Detailed Structure of Turbulent Pulverized Coal Flame by Optical Measurement (Part 2, Instantaneous Two–Dimensional Measurement of Combustion Reaction Zone and Pulverized Coal Particles), JSME Int. J., (2006) (in press).

(16) Hardalupas, Y., Hishida, K., Maeda, M., Morikita, H., Taylor, A.M.K.P. and Whitelaw, J.H., Shadow Doppler Technique for Sizing Particles of Arbitrary Shape, Appl. Opt., Vol.33, No.36 (1994), pp.8417–8426.

(17) Maeda, M, Morikita, H., Prassas, I, Taylor, A.M.K.P. and Whitelaw, J.H., Size and Velocity Measurement by Shadow Doppler Velocimetry within a Pulverized Coal-Fired Furnace, Particle Particle Syst. Characterization, Vol.14 (1997), pp.79–87.

(18) Durst, F., Melling, A. and Whitelaw, J.H., Principle and Practice of Laser-Doppler Anemometry, (1976), Academic Press.

(19) Laser Measurement Handbook, (in Japanese), (1993), pp.159–181, Maruzen Co., Ltd.

(20) Wakabayashi, T., Akamatsu, F., Katsuki, M., Mizutani, Y., Ikeda, Y., Kawahara, N. and Nakajima, T., Development of a Multi-Color Light Collection Probe with High Spatial Resolution (Part1 Evaluation of Spatial Resolution by Ray-Tracing Method), Trans, Jpn. Soc. Mech. Eng., (in Japanese), Vol.64, No.619, B (1998), pp.925–930.

(21) Akamatsu, F., Wakabayashi, T., Tsushima, S., Katsuki, M., Mizutani, Y., Ikeda, Y., Kawahara, N. and Nakajima, T., The Development of Light-Collecting Probe with High Spatial Resolution Applicable to Randomly Fluctuating Combustion Fields, Meas. Sci. Tech., Vol.10 (1999), pp.1240–1246.

(22) Saito, H., Ph.D. Thesis, Osaka University, (in Japanese), (2002).

(23) The Powder Engineering Handbook (The Second Edition), (in Japanese), (1998), pp.36–38, Nikkann Kogyo Shimbun Co., Ltd.
(24) Farzan, H. and Essenhigh, R.H., High Intensity Combustion of Coal, Proc. Combust. Inst., Vol.19 (1982), pp.1104–1111.
(25) Essenhigh, R.H., Misra, M.K. and Shaw, D.W. Ignition of Coal Particles: A View, Combust. Flame, Vol.77 (1989), pp.3–30.